

# An Interaction Potential for Atomic Simulations of Conventional High Explosives

Andrew J. Heim,<sup>1,2</sup> Niels Grønbech-Jensen,<sup>1</sup> Edward M. Kober,<sup>2</sup> Jerome J. Erpenbeck,<sup>2</sup> and Timothy C. Germann<sup>2</sup>

<sup>1</sup>*Department of Applied Science, University of California, Davis, California 95616*

<sup>2</sup>*Theoretical Division, Los Alamos National Laboratory, Los Alamos, New Mexico, 87545*

(Dated: February 2, 2022)

In an effort to develop a chemically reactive interaction potential suitable for application to the study of conventional, organic explosives, we have modified the diatomic AB potential of Brenner *et al.* such that it exhibits improved detonation characteristics. In particular, equilibrium molecular dynamics (MD) calculations of the modified potential demonstrate that the detonation products have an essentially diatomic, rather than polymeric, composition and that the detonation Hugoniot has the classic, concave-upward form. Non-equilibrium MD calculations reveal the separation of scales between chemical and hydrodynamic effects essential to the Zel'dovich, von Neumann, and Döring theory.

## I. INTRODUCTION

For over 15 years, the Reactive Empirical Bond-Order (REBO) potential of Brenner *et al.* [1], or variations thereof, have been used for Molecular Dynamics (MD) simulations of detonation. It has been shown to follow the Chapman-Jouguet (CJ) theory and even that of Zel'dovich, von Neumann, and Döring (ZND) [2]. Being an MD model, it has at least two major shortcomings, namely its spatial and temporal scales. As computers become more powerful and codes and algorithms become more advanced, some of the restrictions that limit these scales can be loosened, allowing for more realistic behavior to be modeled.

While providing an atomic scale model of a reactive material, the empirical and classical model of Brenner *et al.* falls short of including all aspects of an accurate representation. Additionally, the spatial and temporal scales of real explosions make MD simulations a large computational task. But MD is still a useful tool for probing the characteristics of the detonation phenomenon, and the REBO potential is one of the best at balancing realism in the potential with accessibility to the large-scale; yet there is room for improvement.

MD has certain conceptual advantages over hydrodynamics approaches that are parameterized to match the behavior of real high explosives. Even though the latter models can mimic real experiments on the proper spatial and temporal scales, they make assumptions about the reaction rate and multiphase equation of state (EOS) to do so. Some of these assumptions are parameter fittings, which may not elucidate any new physical intuition about detonation of the high explosive (HE) in question. In comparison, MD simulations depend on the parameterization of an interaction potential, which is arguably easier to connect directly to physical considerations than is a multiphase and multi-species EOS.

REBO has been used by many groups to model a variety of parameterizations and experimental configurations. However, a major criticism of this potential is that it has a thin reaction zone ( $\sim 100$  Å) relative to typical real high explosives ( $\sim 1$  mm) [10]. In previous work [3, 4] several unconventional characteristics of the default parameterization of Brenner *et al.* [1] (called ModelI as in [4]) are made evident:

- ModelI displays nearly instantaneous dissociation upon compression by an unsupported detonation. Its entire

reaction zone is characterized by a dissociative state.

- Its reaction zone is thin.
- It readily allows for clustering.
- Its CJ state is highly compressed.
- It has clearly non-hyperbolic equilibrium Hugoniots ( $\mathcal{H}$ ) in  $P$ - $v$  space.

None of these characteristics are proven to be unrealistic. In fact for some primary high explosives, the plasma-like state seen in ModelI at CJ may be realistic [5]. Clustering, particularly of carbon, is a real phenomenon in the thermal decomposition of some HEs [6, 7]. However, successful models of conventional explosives have either assumed or suggested that more molecular states [8, 9] with hyperbolic  $\mathcal{H}$ s in  $P$ - $v$  space [10, 11, 12] are typical and that compressions at CJ conditions should be  $\approx 25\%$  (for example PETN [11]) rather than  $\approx 43\%$  as with ModelI [3]. Given that ModelI can model a dissociated state, it would be useful to show that a more molecular state can also be modeled. The task of this work is to make modifications to the ModelI potential in order to accomplish this goal. Although, for the last feature in the above list, it is difficult to predict what changes would adjust it, an attempt to address the former features is made by making adjustments based on physical reasoning (see Sec. II). In Sec. IV the effects that the changes to the model of Brenner *et al.* have on the thermodynamic properties are investigated by the methods outlined in Sec. III. Notable results of non-equilibrium MD simulations are studied in the companion paper.

## II. CHANGING REBO: PHYSICAL AND AESTHETIC REASONING

In this section we motivate changes to the ModelI potential to form a new potential (called ModelIV after the naming scheme of White *et al.* [4]), the total bonding energy of which takes the form

$$E_b = \sum_i^N \sum_{j>i}^N \{f_c(r_{ij})[(2 - \bar{B}_{ij})V_R(r_{ij}) - \bar{B}_{ij}V_A(r_{ij})] + V_{vdW}(r_{ij})\}. \quad (1)$$

TABLE I: The components and parameters used in Eq. 1.

$$\begin{aligned}
V_R(r) &= \frac{D_e}{S-1} \exp \left[ -\beta \sqrt{2S}(r-r_e) \right] \\
V_A(r) &= \frac{SD_e}{S-1} \exp \left[ -\beta \sqrt{\frac{2}{S}}(r-r_e) \right] \\
B_{ij} &= \left\{ 1 + G \sum_{k \neq i,j} f_c(r_{ik}) \exp[m(r_{ij} - r_{ik})] \right\}^{-n} \\
y(r) &= \frac{r - \gamma_1}{\gamma_2 - \gamma_1} \\
f_c(r) &= \begin{cases} 1 & y(r) < 0 \\ (1 - y(r))^3 (1 + 3y(r) + 6y^2(r)) & 0 \leq y(r) < 1 \\ 0 & 1 \leq y(r) \end{cases} \\
V_{vdW}(r) &= \begin{cases} \epsilon c & r < \alpha_1 \\ \epsilon \left( c + \sum_{i=3}^5 P_i (r - \alpha_1)^i \right) & \alpha_1 \leq r < \alpha_2 \\ \epsilon \left[ \left( \frac{r^*}{r} \right)^{12} - 2 \left( \frac{r^*}{r} \right)^6 \right] & \alpha_2 \leq r < \alpha_3 \\ \epsilon (C_0 + C_1 r + C_2 r^2 + C_3 r^3) & \alpha_3 \leq r < \alpha_4 \\ 0 & \alpha_4 \leq r \end{cases}
\end{aligned}$$

$\text{Mass}_A = 14.008 \text{ amu}$ ;  $\text{Mass}_B = 12.010 \text{ amu}$ ;  $\epsilon = 5.0 \times 10^{-3} \text{ eV}$ ;  $c = 200$ ;  
 $D_e^{AA} = D_e^{BB} = 5.0 \text{ eV}$ ;  $D_e^{AB} = 1.0 \text{ eV}$ ;  $\mathcal{D}_e = D_e + c\epsilon$ ;  $S = 1.8$ ;  
 $\beta = 2.7 \text{ \AA}^{-1}$ ;  $r_e = 1.2 \text{ \AA}$ ;  $G = 5.0$ ;  $m = 2.25 \text{ \AA}^{-1}$ ;  $n = 0.5$ ;  
 $\overline{B}_{ij} = \frac{1}{2}(B_{ij} + B_{ji})$ ;  $\gamma_1 = 1.3 r_e$ ;  $\gamma_2 = 1.7 r_e$ ;  $r^* = 2^{\frac{1}{6}} \times 2.988 \text{ \AA}$ ;  
 $\alpha_2 = 2^{-\frac{1}{6}} r^*$ ;  $\alpha_1 = 0.683 \alpha_2$ ;  $\alpha_3 = \left(\frac{13}{3}\right)^{\frac{1}{6}} r^*$ ;  $\alpha_4 = \frac{67}{48} \alpha_3$ ;  
 $P_3 = -2290.707325617024$ ;  $P_4 = 3603.929410034915$ ;  
 $P_5 = -1513.930039501751$ ;  
 $C_0 = 2.575275778983429$ ;  $C_1 = -4.316677142326428$ ;  
 $C_2 = 1.376573417835169$ ;  $C_3 = -0.12340088128894569$ ;

The parameters for Eq. 1 can be found in Table I. Before mentioning the physical basis for the modifications made to Modell, let us list the features that Modell already takes into account. In tests using Modell, the parameterization is set to a valence of one, which should prefer dimers because one atom's sharing of electrons with one other fills both atoms' valence shells. The bonding energy takes the form

$$E_b = \sum_i^N \sum_{j>i}^N \{ f_c(r_{ij}) [V_R(r_{ij}) - \overline{B}_{ij} V_A(r_{ij})] + V_{vdW}(r_{ij}) \}. \quad (2)$$

See Table I in the errata of Brenner *et al.* [1] for the functions and components of Eq. 2. In Modell this bond-order behavior is implemented by reducing the strength of the attractive term of a Morse potential used to model such covalent bonding. This is accomplished with a bond-order coefficient ( $\overline{B}_{ij}$ ) that varies from one to zero with increasing proximity and number of neighbors.

Rice *et al.* found that Modell allowed for trimer formation and subsequently strengthened this bond-order effect by increasing the repulsive term as well in order to better model bond saturation so that a particle became less likely to bond to more than one other [13, 14]. The contribution of Rice *et al.* is a simplified adjustment for what can be a complicated inter-

action. For instance, the  $\overline{B}_{ij}$  coefficient does not take spin or degeneracy into account. However, this type of correction is similar to the "bond saturation" term that is used in the more sophisticated and calibrated ReaxFF potential of van Duin *et al.* [15].

In combination with this bond-order functionality, the variation of bond well depths allows for reactive chemistry. If  $i$  and  $k$  are different types of atoms, their respective well depths with  $j$  will be different. If  $j$ 's is deeper with  $k$  than with  $i$ ,  $k$  will require less kinetic energy to displace  $i$  than  $i$  would have, had their rolls been reversed. That difference in energy will be converted into the kinetic energy of the system, an exothermic reaction. This is the type of reaction modeled by Modell,  $2AB \rightarrow A_2 + B_2 + 2Q$ , where  $Q \equiv D_e^{AA/BB} - D_e^{AB}$  is the exothermicity of the reaction. The amount of energy needed to dissociate AB is  $D_e^{AB}$ . To dissociate AA or BB requires  $D_e^{AA/BB}$ . These numbers ignore the small contribution of the  $V_{vdW}$  term in Eq. 2.

In Modell the van der Waals (vdW) interaction is represented by a Lennard-Jones (LJ) form. It is connected with a terminating third-order polynomial with negative curvature in the short range domain so that the overly repulsive twelfth-order term does not compete with the Morse potential, which handles the covalent bonding and Pauli Exclusion repulsion. The LJ is parameterized to allow for solid lattice formation at low temperature. It turns out that the third-order inner spline introduces an artifact in Modell since it has a section of positive slope, which allows it to trap particles (see Fig. 1) because of the resulting attractive force. It is only first-derivative continuous at the spline point and is cropped at the cutoff point.

Modell simulates well the repulsion between individual atoms separated by less than their equilibrium distance—which depends on the number and proximity of neighbors to the pair. It does not, however, represent the electrostatic repulsion between dimers that occurs as their charge clouds overlap on approaching each other while still being too far away to rearrange bonds,  $\sim 3 \text{ \AA}$ . As a result there is no significant interaction between molecules at the range and magnitude that gives rise to high pressure dense molecular HE product fluid mixtures [16]. There are some good models for this, for example, ZBL [17] and ReaxFF [15]. In an attempt to improve upon Modell and its results, we design a new model (Model-II), which incorporates, along with the aforementioned contribution of Rice *et al.*, the following modifications:

The inner spline is replaced with a repulsive core, which smoothly connects the negative (the zero of the potential energy is the dissociated state) LJ curve to a constant plateau in the region in which the Morse potential dominates. This inner core has no sections of positive slope—that is, sections of attractive force—and therefore cannot trap atoms, and it crudely models electrostatic repulsion.

The reason for connecting to a plateau is that it allows one to dictate the depth of the bonding potential. It also simplifies the definition of a covalent bond. Any two particles that are within the defined bond distance (see the  $f_c$  term in Table I) with a radial component of kinetic energy less than the height of the plateau are considered bonded. This definition also distinguishes bonded particles from particles that are merely con-

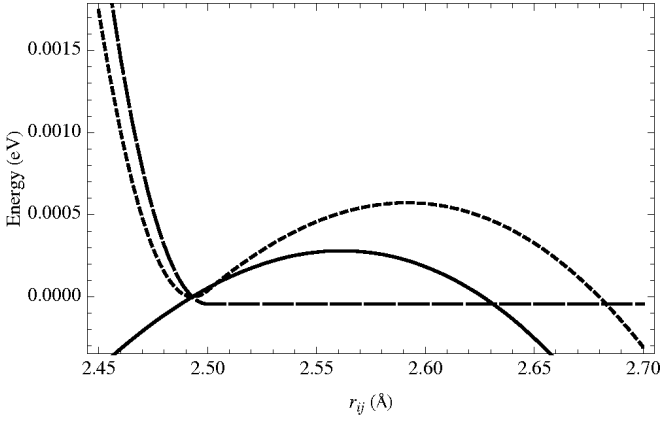


FIG. 1: Total bond energy in a 1D, three-particle, A-B-A, Modell interaction in which the distance between the B and one of the A's is fixed at the bond's equilibrium distance vs. the distance between B and the remaining A (short dash).  $V_{vdW}$  for any two atoms (solid). Total bonding energy less the  $V_{vdW}$  contributions (long dash). All curves are subtracted by their corresponding values at the position of the local minimum of the first curve for comparison purposes. This shows that the section of positive slope in the REBO  $V_{vdW}$  inner spline can trap particles. Without it, there is no trap.

finer by neighbors, and it can be determined at any instant. The height of the plateau, 1 eV, is chosen to be comparable to the thermal energy at the CJ state for Modell [3], an addition that should decrease the reaction cross section, desensitizing the HE to initiation and, perhaps, adjusting reaction time and, thus, the width of the reaction zone. Perhaps, a more physical function would continue to increase monotonically to a finite value at  $r = 0$  and have  $V_{vdW}$  be particle-type dependent.

All of the spline points in ModelIV have, at least, continuous second derivatives, with the exception of the outermost cutoff point. To terminate the  $V_{vdW}$  term in the long range, a Holian–Evans spline [18], which is second derivative continuous at its inner spline point but only first derivative continuous at its outer one, is used. A computational advantage for using the Holian–Evans spline is that the reach of the ModelIV potential is shorter ( $\approx 5.19$  Å) than Modell's ( $\approx 7.32$  Å). Fig. 2 shows a comparison of the two vdW potentials and Fig. 3 shows the corresponding forces. One can see that the ModelIV  $V_{vdW}$  term is still smooth in the force. As with the spline points in the  $V_{vdW}$  term, the cutoff function in the bond-order function and Morse potential is also replaced so that it is second-order continuous. Second derivative continuity helps energy conservation in the MD simulations (and allows longer time steps to be taken).

Another difference between ModelIV and Modell is the depth of the metastable covalent wells. With the addition of the repulsive core, ModelIV fails to detonate with a well as deep as the default value for Modell. The metastable well is raised by 1 eV, such that  $D_e^{AB} = 1.0$  eV,  $D_e^{AA/BB} = 5.0$  eV, and therefore,  $Q = 4.0$  eV. Comparing the potential energy surface for the linear, symmetric, metastable configuration for Modell (see Fig. 4) to the one for ModelIV (see Fig. 5), we notice that the depression near  $(1.2 r_e, 1.2 r_e)$  diminishes

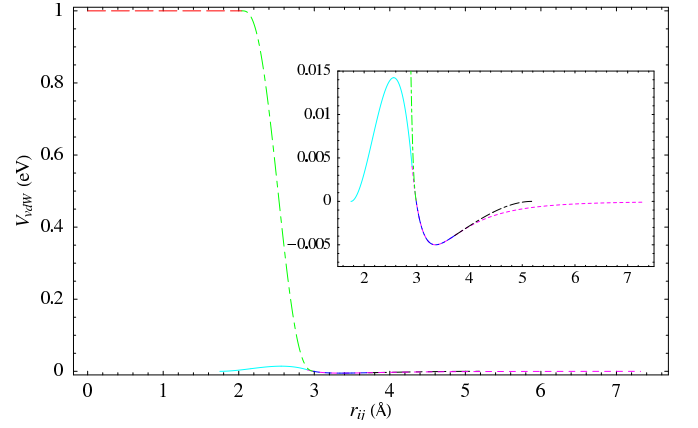


FIG. 2: (Color online) van der Waals ( $V_{vdW}$ ) potential vs. the interatomic distance ( $r_{ij}$ ). Spline points are indicated by changes in color–dashing. Modell  $V_{vdW}$  is made of a third-order polynomial (cyan–solid) connected to a Lennard–Jones (LJ) form (mauve–short dash), which is cropped at a finite distance at which the slope and value of  $V_{vdW}$  are nearly zero. ModelIV  $V_{vdW}$  starts as a constant (red–long dash) and is connected with a fifth-order polynomial (green–long short dashes) so that the spline points are second-derivative smooth, to a LJ form (blue–short short long dashes) at zero, below which it coincides with the Modell LJ until the inflection point, at which it is connected to a curve (black–long long short dashes) that is brought smoothly to zero within a finite distance, a Holian–Evans spline [18].

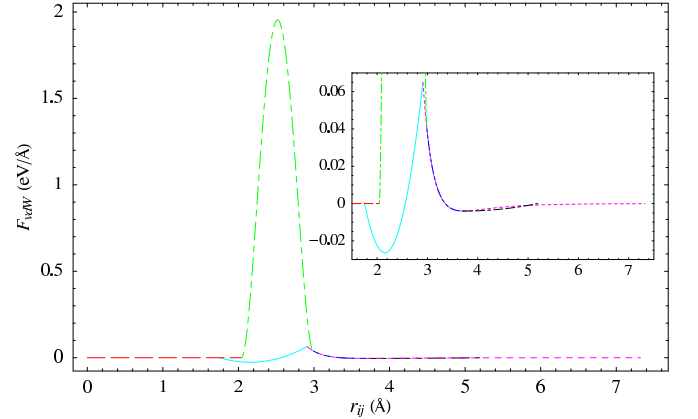


FIG. 3: (Color online) Forces that correspond to the potentials in Fig. 2.

somewhat for ModelIV and that the barrier to be overcome for one particle to displace another via an end-on attack is significantly increased. All of these changes have notable effects on the EOS and detonation properties of the model HE. The final difference is that the masses of the particles are changed so that they are different from each other. The changes to Modell to form ModelIV may be summarized as follows:

- A bond-order coefficient is applied to the repulsive term in the Morse part of the interaction potential.
- The inner spline of the  $V_{vdW}$  term is replaced with a repulsive core, which comprises a plateau connected to

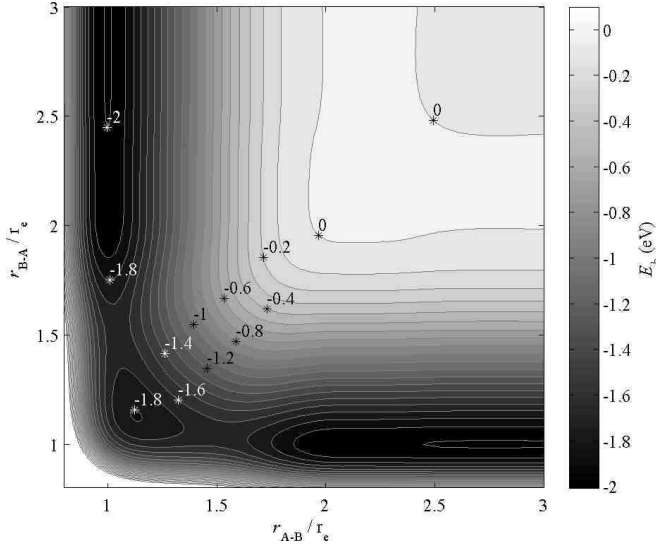


FIG. 4: Potential energy surface for the linear, symmetric, metastable configuration of ModelI atoms. The contours are spaced every 0.1 eV.  $r_{A-B}$  is the distance between A and B atom.  $r_{B-A}$  is the distance between the same A atom and a different B atom.  $r_e$  is the equilibrium distance for the metastable covalent interaction.

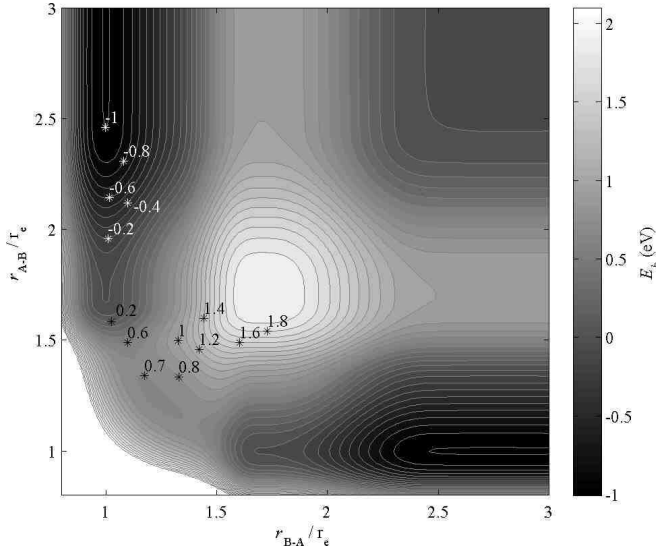


FIG. 5: Potential energy surface for the linear, symmetric, metastable configuration of ModelIV atoms. The contours are spaced every 0.1 eV.

an LJ form with a monotonically decreasing fifth-order polynomial.

- The order of all of the splines is increased such that all but one spline point (the outermost cutoff) have smooth second derivatives.
- The masses of the atom types are changed so that they are no longer equal.
- The depth of the binding energy for the metastable bonds is made shallower.

### III. METHODS

Investigating the two REBO potentials of which this paper is a study, ModelI and ModelIV, we use SPaSM 3.0 [19] to carry out the MD simulations, of which there are two main types, microcanonical ensembles (NVE) and non-equilibrium MD (NEMD). The NVE simulations are used for testing the thermochemical properties of a model and NEMD are used to investigate its detonation behavior. Both utilize the leapfrog Verlet method to advance the atoms' positions and momenta.

We conduct two sub-types of NVE simulations. The first is meant to find the equilibrium Hugoniot and are similar to those described by others [3, 13, 20]. The new model requires a shorter time step  $\delta t \approx 0.16$  fs than does that of Brenner *et al.* [1],  $\delta t \approx 0.25$  fs because of the relatively high curvature of the fifth-order spline in ModelIV's  $V_{vdW}$  term. Its zero-pressure configuration is also slightly different. The length of the sides of the rectangular unit lattice cell are  $l_x = 6.19122$  Å and  $l_z = 4.20538$  Å. The cell contains two dimers in a herringbone configuration. The angles that the dimers make with the horizontal are  $\pm 27.7109^\circ$ . The atoms are placed 0.59976 Å from the centers of their respective dimers, which are positioned at  $(1/4 l_z, 1/4 l_x)$  and  $(3/4 l_z, 3/4 l_x)$  from the lower left corner of the cell. These values are determined by isothermal-isobaric Monte Carlo simulations.

The second type of NVE simulation, the cookoff, is used to determine the reaction rate. The initial conditions are the same as with the first type of NVE except that the constituents are  $100 \times 100$  cells<sup>2</sup> of AB not  $25 \times 25$  of AA and BB. The time step is also drastically reduced so that good statistics can be found for measurements taken during rapid reactions. The time step varies among cookoff simulations,  $6 \times 10^{-4}$  fs  $< \delta t < 0.02$  fs.

One of the purposes of creating a new potential is to expand the reaction zone by lowering the reaction cross section. This requires larger NEMD simulations to be performed. As Rice *et al.* have done [13] for computational efficiency, we try to reduce the amount of pre-shocked material modeled by tacking initial state material onto the end of the sample as the shock front approaches. To reduce surface effects, we introduce at the surface a one-cell-thick layer of two new particles, C and D, that have all of the properties of A and B, respectively, except that they start frozen and their velocities are not updated. When the shock front nears the frozen layer, the frozen layer is converted to A and B and is thermalized along with the new material. Another frozen layer is tacked onto the end. The size of an NEMD simulation is discretely dependent on time. The largest simulation contained over three million atoms.

Another effect of decreasing the reaction cross section is that the incubation time, before which detonation occurs, extends. The sensitivity to impact is thus lessened. To overcome this, we initially overdrive the simulation with a piston that moves into the material at a velocity  $u_{pstin} \approx 4.9$  km/s. After a detonation front has seemingly been established, it is smoothly backed off by following a sine-shaped deceleration over 200 time steps to a desired velocity. The time step is the same as with the first type of NVE simulation,  $\delta t \approx 0.16$  fs. Most of the results of the NEMD simulations are reported in

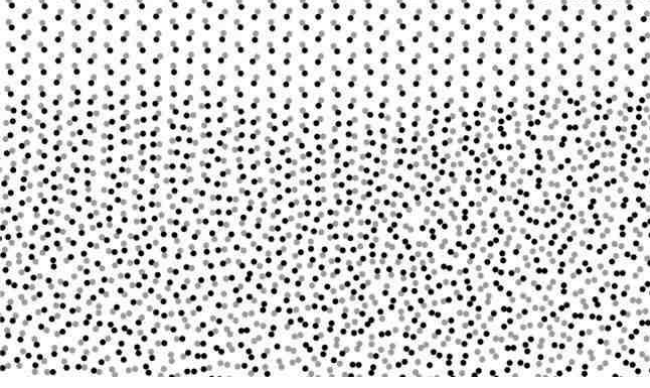


FIG. 6: Snapshot of a section of a shock front for an under-supported detonation using the ModelIV potential. Shock is propagating upward. Particles are shaded by atom type.

the companion paper.

#### IV. COMPARISON OF THERMODYNAMIC PROPERTIES

We start the comparison of the properties of ModelII and ModelIV by analyzing how the ModelIV material behaves when compressed by the passage of an under-driven detonation front. From the snapshot of an NEMD simulation using ModelIV (see Fig. 6), one can see on the left half that many unreacted dimers are lining up horizontally. This is representative of uniaxial compression. Farther back it has melted, and farther back still reacted products are evident. On the right half, the dimers do not seem to line up before reacting. It is made evident in the companion article that this is an effect of detonation instability and the propagation of transverse waves. When comparing this to a snapshot of detonation in ModelII (see Fig. 1 in the paper of Heim *et al.* [3]), one notices that, even at the right side of the sample, ModelIV seems to hold its molecular identity better than ModelII during compression by a detonation front that is not overdriven. It seemingly displays a greater resilience to dissociation. Both the right half of the ModelIV snapshot and the ModelII snapshot lack a significant induction zone.

To better compare the widths of the detonation fronts of the two models, profiles of the average  $z$ -component of particle velocity from a critically supported detonation of ModelIV are plotted. Figure 7 indicates that the reaction zone is about 700 Å wide since that is the position at which the curves settle down to the constant  $u_{pj}$ . With the same method, the width of the reaction zone for ModelII was determined to be about 300 Å [3].

Although ModelIV's reaction zone is still small compared to that of real explosives, it can be widened. To widen the reaction zone farther, one can create a reaction that requires more steps. One also can have the reaction increase the number of moles of material. The resulting expansion in volume would be another driver for the shock wave [2]. Yet another effect of this would be to introduce an entropic penalty to back-reaction and make the model more closely approximate

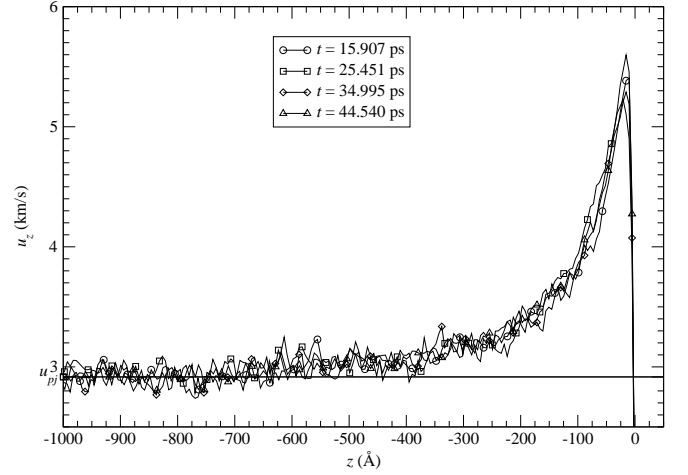


FIG. 7: Overlap of profiles of the  $z$ -component of the particle velocity for a critically supported NEMD simulation using ModelIV parameterized such that  $D_e^{AB} = 1.0$  eV and  $Q = 4.0$  eV. A constant line is drawn at the CJ value of the particle velocity ( $u_{pj}$ ), at which the driving piston is moving. Using a critically supported NEMD as opposed to an unsupported one drastically reduces the transient time from initiation to steady state [3].

TABLE II: Determined thermodynamic values at CJ for ModelIV, where  $v$  is the specific volume,  $u_s$  is the shock velocity,  $u_p$  is the particle velocity,  $T$  is the temperature,  $U$  is the potential energy,  $E$  is the internal energy,  $P$  is the pressure, and  $\lambda$  is the degree of reaction. Subscript  $j$  indicates the CJ value, Subscript 0 indicates the value at the initial state. Averages are per particle.

$v_j/v_0$	0.789851(39)
$u_{sj}$	13.87868(50)
$u_{pj}$	2.91658(44)
$\langle k_B T_j \rangle$ (eV)	0.9185(84)
$\langle U_j \rangle$ (eV)	-0.8631(72)
$\langle E_j \rangle$ (eV)	0.0554(12)
$P_j$ (eV/Å <sup>2</sup> )	0.83846(16)
$\lambda_j$	0.8548516(36)

the ZND assumption of irreversibility.

To find the critical piston velocity in the preceding analysis, the CJ state for ModelIV is found by conducting NVE simulations and seeking the values of  $E$  and  $v$  that satisfy the Hugoniot jump conditions [3, 13, 20]. For ModelII  $v_j/v_0 \approx 0.57$  and  $u_{sj} \approx 9.7$  km/s [3]. From the results (see Table II), one should notice that for ModelIV the CJ state is less compressed than for ModelII and that  $u_{sj}$  is faster. Compared to conventional explosives, which typically have specific volumes  $v_j/v_0 \approx 0.75$  and shock velocities  $u_{sj} \approx 6$  km/s (for example PETN [11]), ModelIV detonation fronts are over twice as fast and its CJ state is slightly less compressed. Note, however, that it has been shown for these REBO potentials that 3D simulations have lower, and therefore more realistic, velocities than do 2D ones [4, 21]. Heim *et al.* [3] show how closely the conditions of the final state in a detonation of a ModelII material match those of the CJ conditions. For contrast in Fig. 8,

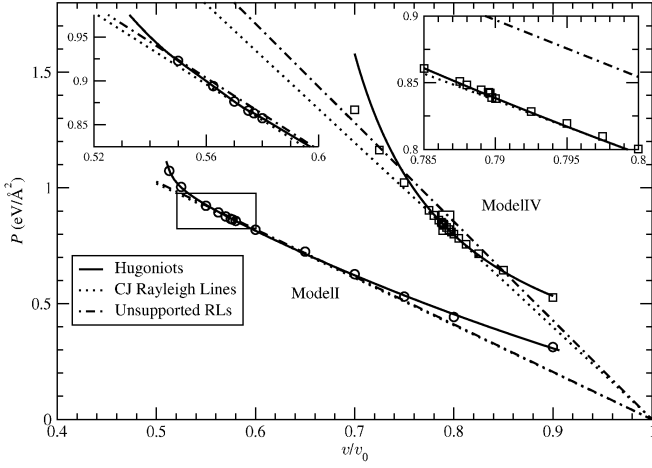


FIG. 8: Hugoniot for ModelII (circles) and ModelIV (squares). Solid lines are a guide to the eye for ModelII and a fit for ModelIV. Rayleigh lines are determined by the initial conditions and slopes. Dotted lines represent Rayleigh lines the slope of which are determined by the CJ value of the detonation velocity. Slopes of dash-dotted lines are determined by the average velocity of the shock waves in unsupported detonations. Boxes are magnifications.

one can see that the Rayleigh line for the unsupported simulation is significantly steeper than for that of the CJ state.

In ZND theory this would require that the final state for ModelIV is either at a strong point or a weak point. The strong point is unstable and will only be a solution to the conservation equations if the detonation is overdriven. In the strict ZND theory there is no path to the weak point. ZND is, however, based on assumptions not realized by ModelIV. ModelIV has a reversible reaction, the pathway of which includes an endothermic dissociation. Endothermic steps can be responsible for weak point final states [2]. Perhaps, the repulsive core introduced in ModelIV, by sheltering the dimers, prevents the reduction of the activation energy of the dissociative step and, hence, increases that step's reaction time, thus making it a stronger contributor to the overall reaction rate and causing the final state to be at a weak point. As is shown in the accompanying paper and can be inferred from Fig. 6, however, a 1D theory is not totally appropriate for this model.

In order to confirm that the modifications to the REBO model in the ModelIV potential do, indeed, maintain a dimerized state, the radial distribution function (RDF) at the CJ state is plotted. In Fig. 9 the CJ state of ModelIV is compared to that of ModelII. From the RDF for ModelIV, one can see that, after the peak at  $r = r_e$ , the curve drops to nearly zero while the analogous region in the RDF of ModelII is closer to unity. This is indicative of a molecular state for ModelIV and a dissociative state for ModelII. From Fig. 10, it is clear that the snapshot of the ModelIV CJ state supports the finding of the corresponding RDF. The snapshot for ModelII shows many more clusters and dissociated atoms.

For these images, a bond is defined for each potential. Two particles,  $i$  and  $j$ , are considered bonded if  $E_{b,ij} + KE_{||,ij} < E_c$  and  $r_{ij} < r_c$ , where  $E_{b,ij}$  is as in Eq. 1 for ModelIV and Eq. 2 for ModelII except that the outer sum is over only  $i$  and  $j$ .

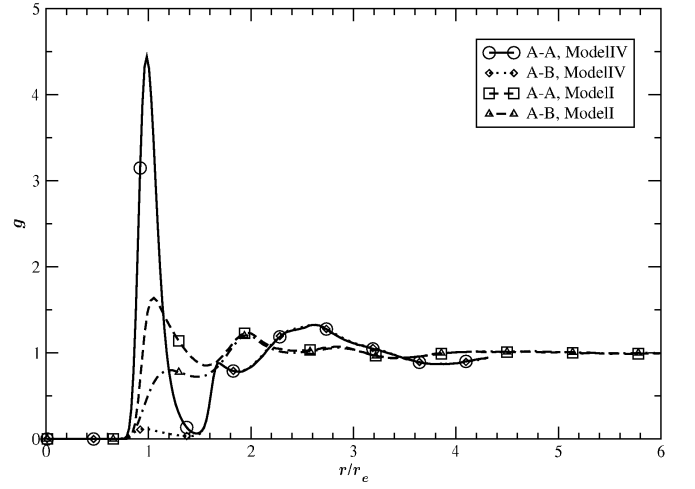


FIG. 9: Radial distribution functions for the CJ states of ModelIV and of ModelII.

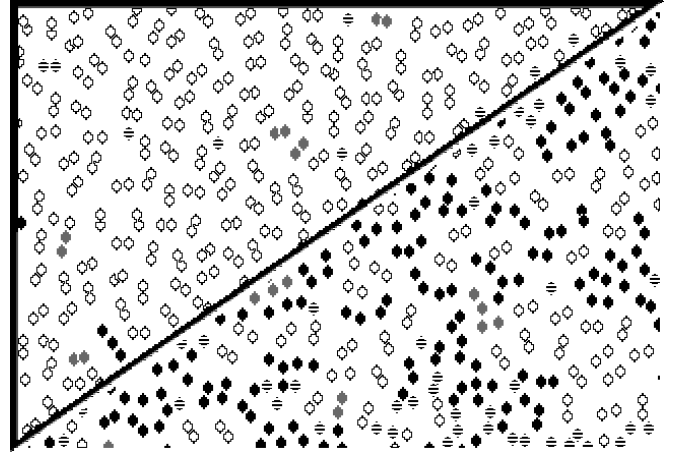


FIG. 10: Snapshots of the CJ state for ModelIV (upper) and ModelII (lower). Particles are marked by bond type. Gray atoms are in unreacted dimers; striped are unbonded, dissociated atoms; black are clustered atoms; and white are reacted dimers.

$KE_{||,ij} \equiv \frac{1}{2}\mu |(\vec{v}_i - \vec{v}_j) \cdot \vec{r}_{ij}/r_{ij}|^2$ .  $\mu$  is the reduced mass of  $i$  and  $j$ . For ModelIV  $E_c = \epsilon c$ , and  $r_c = \gamma_2$  (see Table I). For ModelII  $E_c$  is the peak of the inner spline on the  $V_{vdW}$  term and  $r_c$  is the location of that peak (see Fig. 2). It can be shown that for ModelII there exists no minimum above and within these cutoff values for all values of  $\overline{B}_{ij}$ . To be considered part of a dimer, a particle must be bonded to only one other particle that is bonded to no other. If the particle types are the same, it is a product dimer; if different, a reactant dimer. To be part of a cluster, a particle must be bonded to either multiple particles or to one other that is bonded to multiple particles. To be dissociated, a particle must be bonded to no other.

With a bond defined, cookoffs that will reveal the reaction rate and the activation energy ( $E_a$ ) for each model can be simulated. This is done for two reasons, to compare ModelIV to continuum models and to show another fortuitous difference between ModelII and ModelIV. The cookoffs are NVE simu-

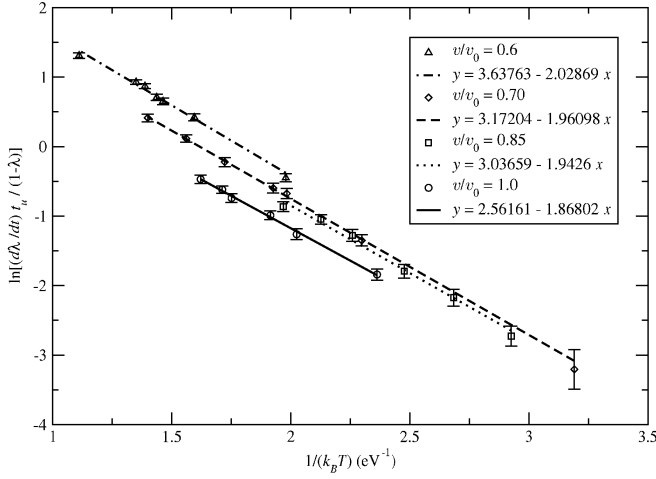


FIG. 11: Reaction rate of ModelIV for various internal energies and volumes vs. temperature. Lines are fits to the Arrhenius form for constant volume. Their slopes are the negative of the activation energy.  $t_u$  is a unit of time and equals 10.180505 fs.

lations started at different values of compression and internal energy but all with the initial AB chemical composition. As a simulation is started, thermal energy is partitioned among the different modes. After this has occurred and the reaction has progressed somewhat, the reaction rate is sampled over a short time and the temporal average of the rate and its standard error are recorded for the current simulation. In Fig. 11 the data are plotted for a series of simulations using the ModelIV potential. For each value of  $v$ , the data are fit to an Arrhenius reaction rate of the form [25]

$$\dot{\lambda} = (1 - \lambda) A \exp \left[ \frac{-E_a}{k_B T} \right], \quad (3)$$

where  $\lambda$  is the degree of reaction defined computationally as the ratio of reacted (defined as above) material to total amount of material.  $\dot{\lambda}$  is the reaction rate and  $A$  is the frequency factor. The analogous plot for ModelII can be found in Fig. 12.

When contrasting the two figures, one notices that, over a similar range of volumes, ModelIV maintains a better fit to the Arrhenius form than ModelII and that the calculation of  $E_a$  remains relatively constant when compared to the  $E_a$  of ModelII. A probable contribution to the former observation is the manner in which a reaction is defined. At compressions typical in detonations, ModelII has a larger number of atoms in clusters and free states, which are not counted as reacted. Only stable dimers are. One may consider a cluster of two A atoms tightly bonded together with a third, B-type particle loosely bonded to one of them as a state more reacted than one in which A is tightly bonded to B and loosely bonded to the other A. However, by our definition of reaction, all particles in a cluster are considered unreacted and only contribute to the denominator of the calculation of  $\lambda$ .

$E_a$  for ModelII decreases with decreasing  $v$ . This is because at higher compressions an atom can have more neighbors within the bonding distance than with ModelIV. The bond-order coefficient then lowers the attraction between it

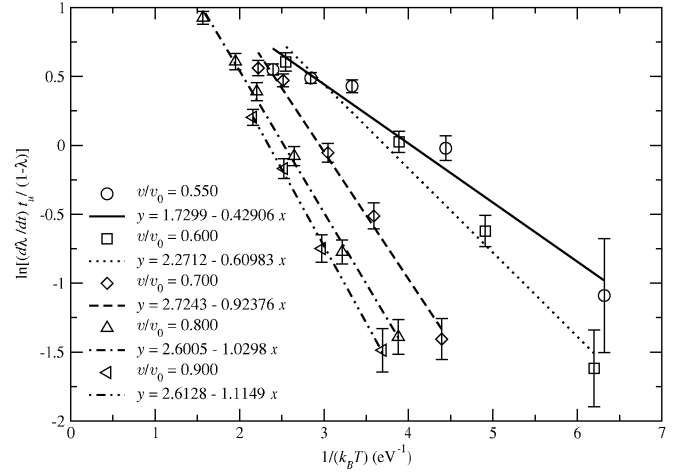


FIG. 12: Reaction rate of ModelII for various internal energies and volumes vs. temperature. Lines are fits to the Arrhenius form for constant volume. Slope is the negative of the activation energy.  $t_u$  is a unit of time.

and its neighbors, making it easier to break apart any existing bonds. For ModelIV, the repulsive core keeps neighbors away from dimers so that the bond-order coefficient and, thus, the dissociation energy remain unaffected by the same level of compression that would otherwise cause ModelII's dissociation energy to be reduced. For ModelIV there is a higher tendency than for ModelII for the compression to use up the space between dimers than that between the dimers' constituents. This is because for the former case a third particle would have to climb the repulsive core that was added to the  $V_{vdW}$  term before it got within the range of the cutoff function  $f_c$ , where it can diminish the bond-order coefficient  $\bar{B}_{ij}$ . In the latter case a third particle would only need to overcome the barrier of ModelII's inner spline (see Fig. 2), which is small compared to the temperature for most situations considered in reaction and detonation. For ModelIV the activation energy goes up slightly with decreasing volume. The exact reason for this is not known at present, but simulations with ReaxFF on the high explosive RDX also show this trend [22].  $E_a$  for ModelIV is roughly 1 eV greater than for ModelII. This is commensurate with the height of the repulsive core.

Even though we show that ModelIV fits an Arrhenius reaction rate in NVE cookoff simulations, we would like to know that this is the type of reaction that takes place in the reaction zone. We can use that reaction rate along with the von Neumann spike (vNs) state to predict a  $\lambda$  profile. Since we do not have the full EOS throughout the reaction zone, we make some assumptions that will tend to shorten the width of the profile. Let's assume that  $u_p$  increases linearly and that  $v$  and  $P$  are constant such that  $T(\lambda)$ . We conduct a series of shock tube simulations of a substance similar to ModelIV except that  $Q$  is set to zero. We find the value of piston velocity that produces the constant zone the state of which falls on the theoretical  $\mathcal{R}$  from Fig. 8. This is the vNs state. The value of the specific volume at the vNs state is  $v_n \approx 0.558 v_0$  and temperature  $T_n \approx 0.25/k_B$ . From Fig.11, we estimate

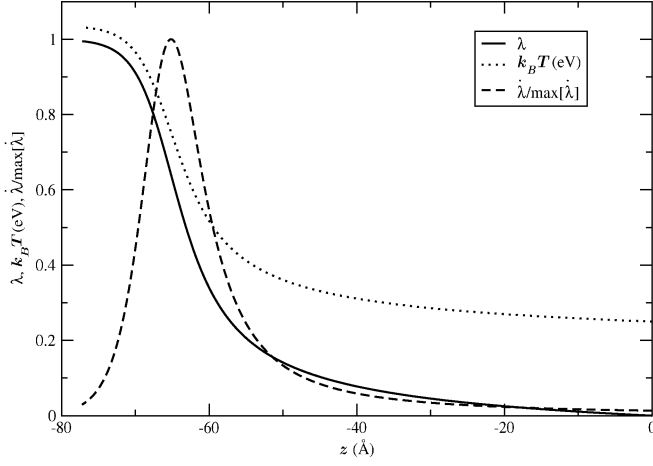


FIG. 13: Theoretical profiles for the degree of reaction ( $\lambda$ ), temperature ( $T$ ), and reaction rate ( $\dot{\lambda}$ ) for ModelIV, assuming a constant pressure and density.  $\max[\dot{\lambda}] = 8.94$  THz.

the reaction rate parameters (see Eq. 3) at the vNs state to be  $A_n \approx 3.6$  and  $E_{an} \approx 2.0$ . Inserting the following equation for temperature

$$T(\lambda) = T_n + (T_j - T_n) \frac{\lambda}{\lambda_j} \quad (4)$$

into Eq. 3 and using the change of variable

$$\frac{d\lambda}{dz} = \frac{d\lambda}{dt} \frac{dt}{dz} = \dot{\lambda} \left( u_{sj} - \frac{u_{pj}}{2} \right)^{-1}, \quad (5)$$

we generate a profile by iterating backward in space via a third order Runge–Kutta method (see Fig.13). The variables with the subscript  $j$  are the CJ values listed in Table II.

The theoretical  $\lambda$  profile reaches  $\lambda_j$  at  $z \approx -70$  Å, much closer to the front than the  $-700$  Å that we measure for the CJ value of the particle velocity in Fig. 7. This does not prove that the reaction rate is Arrhenius in the reaction zone, but it does show that the order of magnitude of the measured reaction zone width is significant compared to the lower bound of the theoretical width. Had it been otherwise, this would have shown the reaction rate to not be Arrhenius and thus a different form, for example, a flame front.

Replacing the assumptions in the analysis with more accurate ones, for example, variable  $v$ , would tend to lengthen the theoretical width because the expansion of the material would tend to cool it and slow the reaction rate. In lieu of the full EOS, we could have used data from an NEMD to fill in the state within the reaction zone. However, we would only be testing internal consistency. This comparison also suffers from an assumption of steady-state one-dimensionality. We have seen that the NEMD simulations are 2D. As we show in the companion paper, transverse waves traverse the reaction zone. This causes the profile to be time and  $x$  dependent. The

EOS throughout the reaction zone is currently being calculated for normal mode stability analysis [24], which assumes an Arrhenius reaction rate.

## V. CONCLUSION

In this paper it was shown that the changes to the ModelII version of the REBO potential have reduced the amount of clustered and dissociated atoms at the CJ state (by RDF) if not throughout the reaction zone (by a snapshot of an NEMD simulation). The CJ state of ModelIV is at a less compressed state and ModelIV's reaction zone is wider than ModelII's is. ModelII's unsupported detonation velocity is much better predicted by CJ theory, where ModelIV's propagates significantly faster. In the companion paper we investigate ModelIV's relative disparity more closely. The cookoff simulations reveal that ModelIV fits an Arrhenius reaction rate through a wider domain of compressions than does ModelII and it has a higher and less density-dependent activation energy.

It was put forth that this higher  $E_a$  causes the final state to be at a weak point since it might make more significant in the reaction rate the endothermic step of dissociation. Given, however, the 2D shape of the front in Fig. 6, such a 1D explanation is probably insufficient. Higher  $E_a$ s should increase the likelihood of 1 and 2D instabilities in detonation waves [23, 24]. The current value of  $\approx 2$  eV is consistent with the presumed activation energies for many conventional HEs.

The goal of the current research is the improvement of REBO, which we believe we have achieved, mainly, by introducing increased atomic repulsion, which reduces the reaction cross section. It was shown that ModelIV's reaction zone is wider than with ModelII and that the CJ state is a molecular one. REBO's insensitivity to initiation is increased, and a thicker induction zone is introduced. The reaction rate now behaves in a more Arrhenius manner, and the product EOS behaves more like a polytropic gas as indicated by the hyperbolic shape of its equilibrium  $\mathcal{H}$ . Some measurements, for example, the adiabatic  $\gamma$ —as is shown in the companion paper—and the amount of compression at CJ, are more commensurate with conventional explosives [10]. However, some are not too close, for example, the reaction temperature and shock velocity. 3D simulations are needed to investigate how the changes truly compare to real experiments.

## Acknowledgments

The authors would like to thank Sam Shaw, Alejandro Strachan, Brad Holian, Tommy Sewell, Yogesh Joglekar, and David Hall for useful conversations. This material was prepared by the University of California under Contract W-7405-ENG-36 and Los Alamos National Security under Contract DE-AC52-06NA25396 with the U.S. Department of Energy. The authors particularly wish to recognize funding provided through the ASC Physics and Engineering Modeling program.



- 
- [1] D. W. Brenner, D. H. Robertson, M. L. Elert, and C. T. White, Phys. Rev. Lett. **70**, 2174 (1993); **76**, 2202(E) (1996).
  - [2] W. Fickett and W. C. Davis, *Detonation* (University of California Press, Berkeley, 1979).
  - [3] A. J. Heim, N. Grønbech-Jensen, T. C. Germann, E. M. Kober, B. L. Holian, and P. S. Lomdahl, Phys. Rev. E **76**, 026318 (2007).
  - [4] C. T. White, D. R. Swanson, and D. H. Robertson, in *Chemical Dynamics in Extreme Environments*, edited by R. A. Dressler (World Scientific, Singapore, 2001), p. 547.
  - [5] D. Heflinger, I. Bar, T. Ben-Porat, G. Erez, and S. Rosenwaks, J. Appl. Phys. **73**, 2138 (1993).
  - [6] X. Tao, X. Kang, and Z. Jiaheng, Mat. Sci. Eng. **B38**, L1 (1996).
  - [7] N. R. Greiner, D. S. Phillips, J. D. Johnson, and F. Volk, Nature **333**, 440 (1988).
  - [8] L. E. Fried and P. C. Souers, Propellants, Explosives, Pyrotechnics **21**, 215 (1996).
  - [9] W. M. Howard, L. E. Fried, and P. C. Souers, in *Eleventh Symposium (International) on Detonation* (1998).
  - [10] C. L. Mader, *Numerical Modeling of Detonations* (University of California Press, Berkeley, 1979).
  - [11] F. H. Ree, J. Chem. Phys. **81**, 1251 (1984).
  - [12] G. L. Schott, M. S. Shaw, and J. D. Johnson, J. Chem. Phys. **82**, 4264 (1985).
  - [13] B. M. Rice, W. Mattson, J. Grosh, and S. F. Trevino, Phys. Rev. E **53**, 611 (1996).
  - [14] B. M. Rice, W. Mattson, J. Grosh, and S. F. Trevino, Phys. Rev. E **53**, 623 (1996).
  - [15] A. C. T. van Duin, A. Strachan, S. Stewman, Q. Zhang, X. Xu, and I. William A. Goddard, J. Phys. Chem. **107**, 3803 (2003).
  - [16] M. S. Shaw, private communication.
  - [17] J. F. Ziegler, J. P. Biersack, and U. Littmark, *The Stopping and Ranges of Ions in Solids, Vol. I* (Pergamon, 1985).
  - [18] B. L. Holian and D. J. Evans, J. Chem. Phys. **78**, 5147 (1983).
  - [19] P. S. Lomdahl, P. Tamayo, N. Grønbech-Jensen, and D. M. Beazley, in *Proceedings of Supercomputing 93* (IEEE Computer Soc Press, Los Alamitos, CA, 1993), p. 520.
  - [20] J. J. Erpenbeck, Phys. Rev. A **46**, 6406 (1992).
  - [21] J.-B. Mailliet, B. Crouzet, C. Matignon, L. Mondelain, and L. Soulard, in *Shock Compression of Condensed Matter - 2003* (AIP, 2004), vol. 706, pp. 385–388, <http://link.aip.org/link/?APC/706/385/1>.
  - [22] A. Strachan, E. M. Kober, A. C. T. van Duin, J. J. Oxgaard, and W. A. Goddard, J. Chem. Phys. **122**, 54502 (2005).
  - [23] H. I. Lee and D. S. Stewart, J. Fluid Mech. **216**, 103 (1990).
  - [24] M. Short and D. S. Stewart, J. Fluid Mech. **368**, 229 (1998).
  - [25]  $(\lambda_e - \lambda)$  makes a more accurate coefficient, where  $\lambda_e$  is the equilibrium value of  $\lambda$  and could be a source of further temperature and density dependence.